Journal of Mines, Metals and Fuels, *73(6): 1637-1650; 2025. DOI: 10.18311/jmmf/2025/48768*

Print ISSN : 0022-2755

Journal of Mines, Metals and Fuels

Contents available at: *www.informaticsjournals.co.in/index.php/jmmf*

Stress and Strain Distribution Patterns Around Centrally Elongated Notch in Flat Plate

Vinayak H. Khatawate[1]*, M. A. Dharap[2], Hari Vasudevan[1], V. G. Balikai[3] and P. P. Revankar[3]

[1]Department of Mechanical Engineering, SVKM's Dwarkadas J. Sanghvi College of Engineering, Vile Parle, Mumbai - 400056, Maharashtra, India; vinayak.khatawate@djsce.ac.in

[2]Department of Mechanical Engineering, Veermata Jeejabai Technological University, Mumbai - 400019, Maharashtra, India

[3]School of Mechanical Engineering, KLE Technological University, Hubli - 580031, Karnataka, India

Abstract

Industries such as aerospace, automotive, civil engineering, and consumer and industrial goods increasingly rely on Finite Element Analysis (FEA) as an essential part of their design processes. In these fields, localised Stress Concentrations (SC), caused by features like steps, notches, or discontinuities, play a significant role in determining the mechanical performance of components. These irregularities generate areas where stress significantly exceeds the average stress in the surrounding material, raising critical concerns under external loads. Such high-stress zones can increase strain and potential failure modes, including cracking or fatigue, which are particularly concerning in applications requiring durability and reliability. This study examines elastic stresses and strains in a flat plate with centrally elongated notches of varying geometries. Using FEA, the analysis focused on a plate subjected to longitudinal tension, evaluating the effects of Poisson's ratio (μ) values ranging from 0.15 to 0.49 and notch Depth ratios (r/D) from 0.2 to 1. The results showed that even under elastic conditions, the Stress Concentration Factor (SCF) and the Strain Concentration Factor (SNCF) varied due to the influence of μ. Poisson's ratio significantly affected the SNCF, highlighting the importance of accounting for these factors to ensure structural reliability in components with geometric discontinuities.

Major Findings: *This study analyses elastic stresses and strains in a notched flat plate under longitudinal tension using FEA. It examines the effects of Poisson's ratio (0.15-0.49) and notch depth ratio (0.2-1) on stress and strain concentration factors. The findings highlight Poisson's ratio's significant impact on SNCF, emphasising its role in structural reliability.*

Keywords: *Finite Element Analysis (FEA), Notch, Poisson's Ratio, Strain Concentration Factor (SNCF), Stress Concentration Factor (SCF)*

1.0 Introduction

Structural components and engineering elements frequently include irregularities like steps, notches, or geometric discontinuities. These features create localised stress or strain concentrations when subjected to external loads. Such SC sites can significantly reduce the structural lifespan under service conditions, as cracks often originate in these regions. Pilkey[1] and Young[2] provide comprehensive tables and diagrams detailing SCFs for a wide variety of specimen geometries.

However, many readily available SCF references, primarily based on two-dimensional elastic solutions, tend to overlook the influence of Poisson's ratio (μ) on SC. In contrast, three-dimensional theoretical models or FEA[3–8] have been used to study notch fields along the thickness of notches and holes. For both 2D and 3D scenarios, stress and strain concentration parameters can

**Author for correspondence*

vary based on material properties[9]. Poisson's ratio (μ) affects SCFs and SNCFs by influencing the distribution of stress, strain, and volume changes within the material. Specifically, for configurations such as a circular hole at the centre of a plate or semicircular notches along its opposite edges under tensile loading, SCF depends on μ[10,11]. Even within the elastic range, SCFs and SNCFs are not constant. While some studies[12–14] address the effect of μ on SC, they often neglect its impact on SNCFs in plates with centrally elongated notches of varying depths on opposite edges.

This study employs FEA to investigate the combined effects of geometric configurations and μ on the SCF and SNCF of flat plates. The analysis focuses on plates with centrally elongated notches of varying ligament depths. A comparison of FEA results with existing analytical solutions[15,16] validates the findings. The study's main goal is to distinguish between the stress concentration factor (K_σ) and the strain concentration factor (K_ε). Furthermore, it aims to evaluate the influence of μ on SCFs and SNCFs in plates featuring centrally elongated notches.

2.0 Modelling Strategies and Computational Methodologies

2.1 Definition of the Problem

A plate with finite thickness and centrally placed elongated notch was analysed under tensile loading, as demonstrated in Figure 1. The plate's geometry is defined by its thickness t, width W, and height H. The radius of the semicircular notch is denoted as r, while D/2 represents the distance from the notch roots to the plate's edge. The parameter t1 signifies half the notch length aligned parallel to W. The material is assumed to be elastic, homogeneous, and isotropic. The analysis is conducted using rectangular coordinates (x,y,z).

The definitions of the stress and strain ratios are, respectively:

$$k_\sigma = \frac{\sigma_{yy}}{\sigma_{net}} \quad \text{and} \quad k_\varepsilon = \frac{\varepsilon_{yy}}{\varepsilon_{net}} \tag{1}$$

The SCF K_σ is

$$K_\sigma = \frac{\sigma_{yy0}}{\sigma_{net}} \tag{2}$$

The SNCF K_ε is

$$K_\varepsilon = \frac{\varepsilon_{yy0}}{\varepsilon_{net}} \tag{3}$$

Where,

$$\sigma_{net} = (\sigma_{y0} W/D) \text{ and } \varepsilon_{net} = (\sigma_{y0} W/ED).$$

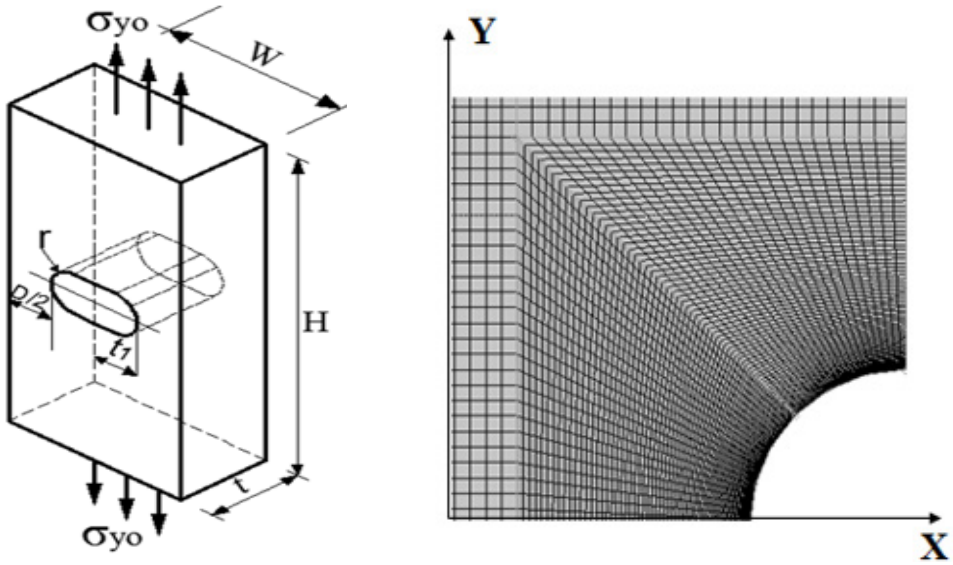


Figure 1. Geometry and the FEA meshed model.

In the vicinity of the notch root, two constraint parameters, viz., out of plane (T_z) and in-plane (T_x) SCF is used to describe 3D characteristics of the stress fields.
The out-of-plane stress constraint factor is

$$T_z = \frac{\sigma_{zz}}{\sigma_{xx}+\sigma_{yy}} \quad (4)$$

and the in-plane stress factor is

$$T_x = \frac{\sigma_{xx}}{\sigma_{yy}} \quad (5)$$

$T_z = 0$ for the plane stress state and $T_z = \mu$ for the plane strain state. For the finite thickness plate of elastic material, $0 \le T_z \le \mu$, μ is the Poisson's ratio of the material.

2.2 Finite Element Mesh and Convergence Evaluation

Figure 1 illustrates the meshed model employed in the study. The FEA was conducted using HYPERWORKS[17] software. Considering symmetry, only one-fourth of the model was analysed, with suitable symmetrical boundary conditions applied. The flat plate's dimensions included a height (H) of 80mm, a width (W) of 40mm, and a thickness (t) of 5mm. The notch depth-to-diameter ratio (r/D) ranged from 0.2 to 1, corresponding to distances (D) between 25mm and 5mm. The Poisson's ratio (μ) was varied from 0.15 to 0.49. The reason for varying the values of Poisson's ratio is mainly to consider the effect of μ on the notch configuration A uniform load of 2000N, equivalent to a stress of 20MPa, was applied along the plate's boundary. Plane stress conditions were assumed since the plate's thickness was much smaller than its other dimensions. Eight-node quadrilateral shell elements were utilised for the analysis, with a finer mesh near the notch root to accurately capture variations in stress and strain fields. Convergence tests were performed for all r/D ratios to ensure the reliability and stability of the results, as depicted in Figure 2.

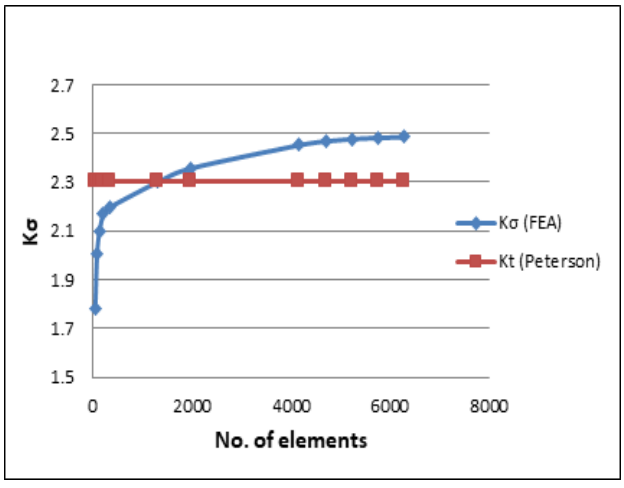


Figure 2. Convergence of meshing for *r/D=0.667*.

3.0 Distribution Patterns of and Around the Notch Root

Variations in stress and strain near the notch root are represented by k_σ and k_ε. Figures 3 and 4 illustrate their dependence on r/D and μ. Here, x denotes the distance from the notch root, and D is the ligament length ahead of the notch tip. Both k_σ and k_ε decrease as x increases. While μ has minimal impact on the stress ratio k_σ distribution at or near the notch root, it significantly influences the strain ratio (k_ε) distribution (Figure 3), although this effect lessens with increasing x. Higher values of μ result in increased strain ratios near the notch root. Shallow notches (r/D=0.2, 0.25) exhibit higher k_σ and k_ε values at the notch root compared to deeper notches (r/D=1, 0.5), as shown in Figure 4. The values of k_σ and k_ε at the notch root are inversely proportional to the notch depth (r/D). Moreover, the k_σ–x/(D/2) and k_ε–x/(D/2) curves become flatter as D decreases. Figures 3 and 4 provide a detailed

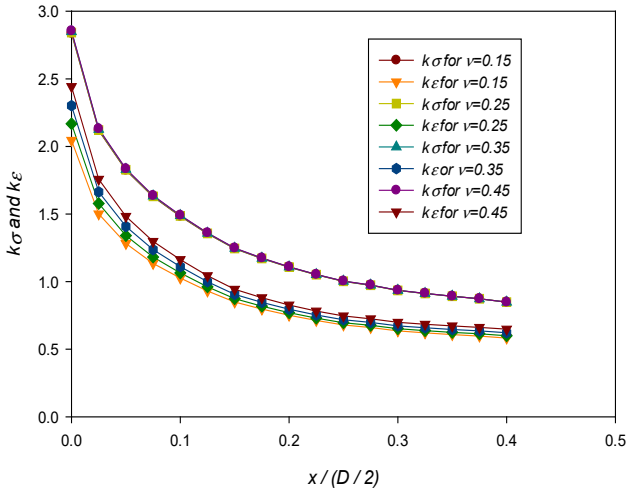


Figure 3. The distribution of k_ε and k_σ for different μ (at r/D=0.2).

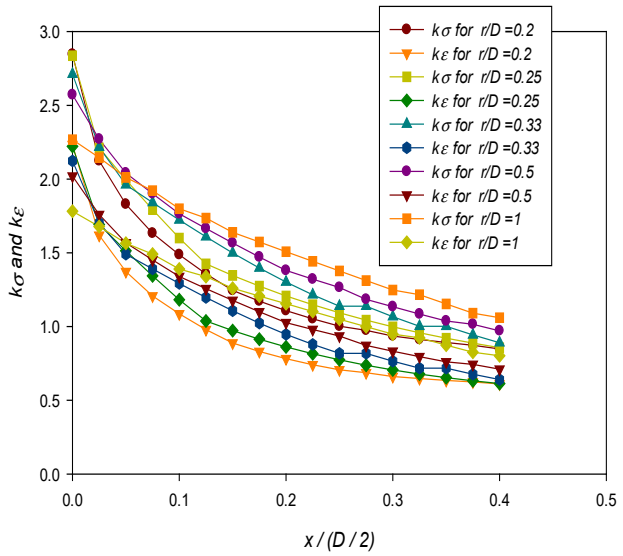


Figure 4. The distribution of k_ε and k_σ for different r/D (at μ=0.3).

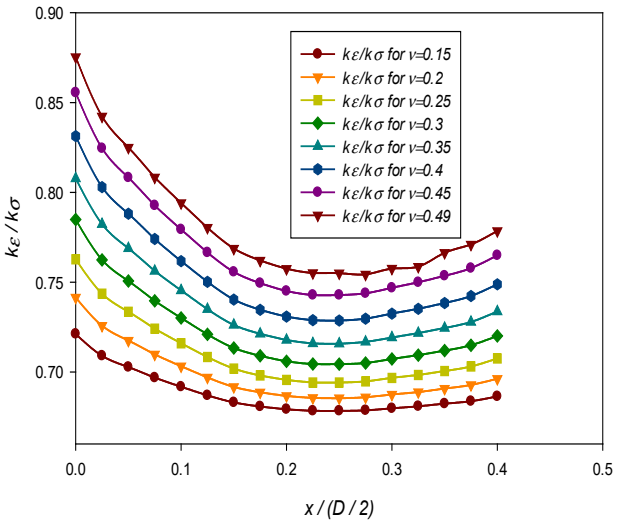


Figure 5. The distribution of (k_ε /k_σ) near the notch root for various μ (at r/D=0.2).

visualisation of the distributions of k_σ and k_ε near the notch root for different μ and r/D values.

The distribution of k_ε/k_σ near the notch is shown in Figures 5 and 6 for various μ and r/D values, with notable distinctions between the behaviour of k_ε and k_σ across the plate. The distribution of k_ε differs from the k_σ within the plate. Near the notch root, both at and ahead of it, the ratio k_ε /k_σ increases as μ rises (Figure 5). Table 1 provides a summary of the k_ε /k_σ distribution near the

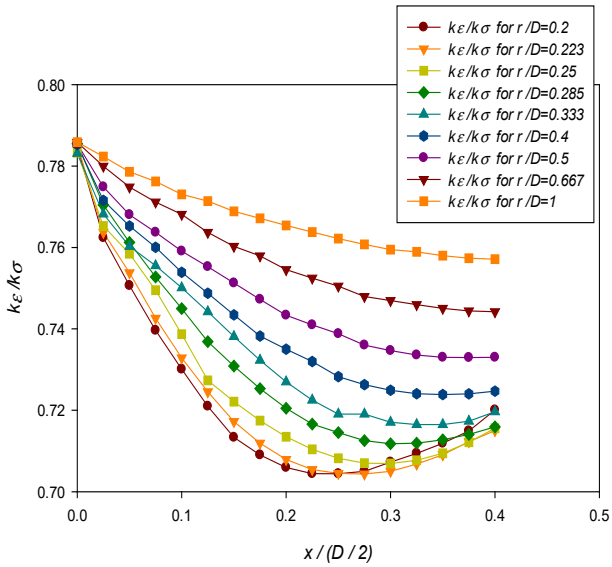


Figure 6. The distribution of (k_ε /k_σ) for different r/D (at μ=0.3).

notch root for various μ values when r/D=0.2. At the notch root (x/(D/2)=0), the percentage change in k_ε /k_σ for μ = 0.25, 0.35, and 0.45 relative to μ=0.15 is −5.76%, −12%, and −5.76%, respectively. At x/(D/2)=0.2 and 0.4, the variations are −2.4%, −5.67%, −9.68% and −3.07%, −6.88%, −11.43%, respectively. This trend indicates that the variation in k_ε /k_σ for different Poisson's ratios decreases up to x/(D/2)=0.25 as x increases, but increases again beyond this point. Additionally, the k_ε/k_σ the ratio varies across different regions of the plate.

As depicted in Figure 6, the k_ε /k_σ distribution remains nearly constant at the notch root, regardless of changes in notch depth (r/D). For notch depths of r/D=0.25, 0.285, 0.33, 0.4, and 0.5, the k_ε/k_σ ratio decreases up to x/(D/2)=0.3, 0.325, 0.35, 0.375, respectively, before rising again.

The k_ε /k_σ versus x/(D/2) distribution for different μ and r/D values does not exhibit a consistent decrease with distance from the notch root. The value of μ significantly affects the shape of the k_ε /k_σ-x/(D/2) curve across all locations along the plate (Figure 5). While the notch depth (r/D) influences the k_ε/k_σ-x/(D/2)) curve at all points except the notch root, variations in k_ε /k_σ are determined by μ, r/D, and the position within the plate. Moreover, it is observed that k_ε is smaller than k_σ in regions of stress or strain concentration.

Table 1. The distributions of k_ε / k_σ near the notch root for different μ values

x/ (D/2)	k_ε / k_σ (For μ = 0.15)	k_ε / k_σ (For μ = 0.2)	k_ε / k_σ (For μ = 0.25)	k_ε / k_σ (For μ = 0.3)	k_ε / k_σ (For μ = 0.35)	k_ε / k_σ (For μ = 0.4)	(For μ = 0.45)	k_ε / k_σ (For μ = 0.49)	% variation of k_ε / k_σ for μ = 0.25 from μ = 0.15	% variation of k_ε / k_σ for μ = 0.35 from μ = 0.15	% variation of k_ε / k_σ for μ = 0.45 from μ = 0.15
0	0.7212	0.7415	0.7628	0.7849	0.8078	0.8313	0.8555	0.8754	-5.7641	-12.0052	-18.6263
0.025	0.7090	0.7258	0.7436	0.7624	0.7823	0.8030	0.8246	0.8423	-4.8757	-10.3354	-16.2929
0.05	0.7028	0.7175	0.7336	0.7507	0.7689	0.7881	0.8082	0.8250	-4.3831	-9.4079	-15.0063
0.075	0.6969	0.7098	0.7241	0.7396	0.7563	0.7740	0.7927	0.8084	-3.9156	-8.5253	-13.7538
0.1	0.6918	0.7032	0.7160	0.7301	0.7454	0.7618	0.7793	0.7941	-3.5009	-7.7522	-12.6541
0.125	0.6870	0.6970	0.7084	0.7210	0.7350	0.7502	0.7665	0.7804	-3.1069	-6.9823	-11.5783
0.15	0.6831	0.6917	0.7019	0.7134	0.7262	0.7403	0.7557	0.7687	-2.7529	-6.3054	-10.6281
0.175	0.6808	0.6887	0.6981	0.7090	0.7213	0.7346	0.7495	0.7621	-2.5335	-5.9439	-10.0822
0.2	0.6793	0.6867	0.6956	0.7060	0.7178	0.7309	0.7451	0.7575	-2.4097	-5.6746	-9.6878
0.225	0.6784	0.6856	0.6942	0.7045	0.7159	0.7289	0.7429	0.7551	-2.3267	-5.5298	-9.4965
0.25	0.6784	0.6854	0.6942	0.7044	0.7158	0.7287	0.7429	0.7550	-2.3240	-5.5125	-9.5028
0.275	0.6787	0.6860	0.6948	0.7050	0.7168	0.7297	0.7438	0.7543	-2.3781	-5.6180	-9.5980
0.3	0.6798	0.6875	0.6968	0.7073	0.7192	0.7325	0.7469	0.7576	-2.4933	-5.7946	-9.8659
0.325	0.6809	0.6888	0.6984	0.7094	0.7217	0.7352	0.7500	0.7586	-2.5652	-5.9885	-10.1395
0.35	0.6824	0.6908	0.7006	0.7119	0.7245	0.7384	0.7535	0.7664	-2.6637	-6.1736	-10.4271
0.375	0.6838	0.6928	0.7031	0.7149	0.7279	0.7423	0.7578	0.7710	-2.8239	-6.4487	-10.8321
0.4	0.6864	0.6963	0.7076	0.7201	0.7337	0.7489	0.7649	0.7785	-3.0780	-6.8831	-11.4347

4.0 The Distributions of SCF ($K_{\sigma L}$) and SNCF ($K_{\varepsilon L}$) at Notch Root

An overview of SCF and SNCF distributions using FEA is provided in this section, including the linear elastic SCF, often described as the theoretical SCF. The linear elastic SCF is defined as "the ratio of the maximum stress at the notch root to the nominal stress" and is widely utilised in both industry and academia to quantify stress concentration around geometric discontinuities. Initial estimates of SCFs for various notch configurations were experimentally obtained using photoelasticity, as documented in references[18,19]. References[1,2] include curves and empirical formulas for determining SCF in different notched bars, focusing exclusively on SCFs without considering SNCFs. This study highlights the distinction between SCF and SNCFs and shows that μ significantly affects both SCF and SNCFs when evaluating stress concentrations in notched bars.

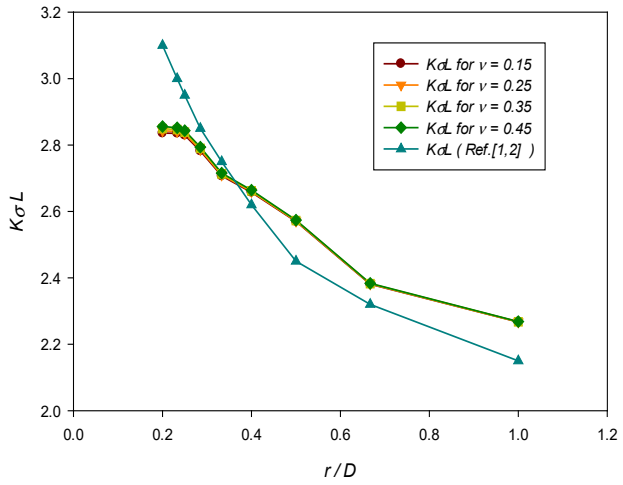


Figure 7. Distribution of SCF ($K_{\sigma L}$) with r/D for different μ.

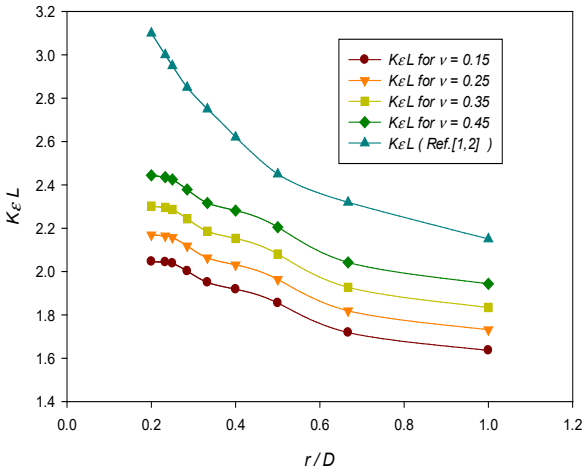


Figure 8. Distribution of SNCF ($K_{\varepsilon L}$) with r/D for different μ.

Table 2. Distributions of the $K_{\sigma L}$ at the notch root for different μ

r/D	$K_{\sigma L}$ For μ = 0.15	$K_{\sigma L}$ For μ = 0.25	$K_{\sigma L}$ For μ =0.35	$K_{\sigma L}$ For μ =0.45	$K_{\sigma L}$ (Ref. [1,2])	% variation of Ref. [1,2] from FEA for μ = 0.15	% variation of Ref. [1,2] from FEA for μ = 0.45
0.2	2.83601	2.84298	2.84947	2.85584	3.10000	-9.30862	-8.54966
0.233	2.83525	2.84108	2.84670	2.85221	3.00000	-5.81066	-5.18150
0.25	2.82957	2.83440	2.83906	2.84362	2.95000	-4.25599	-3.74085
0.285	2.78217	2.78618	2.79003	2.79377	2.85000	-2.43796	-2.01285
0.333	2.70708	2.71006	2.71296	2.71581	2.75000	-1.58561	-1.25897
0.4	2.65791	2.66007	2.66216	2.66423	2.62000	1.42615	1.66010
0.5	2.56990	2.57139	2.57284	2.57426	2.45000	4.66550	4.82691
0.667	2.38076	2.38166	2.38251	2.38334	2.32000	2.55222	2.65774
1	2.26679	2.26728	2.26774	2.26820	2.15000	5.15229	5.21098

The variation of $K_{\sigma L}$ and $K_{\varepsilon L}$ at the notch root with respect to r/D for various μ values is illustrated in Figures 7 and 8. As shown, the SCF and SNCFs decrease with increasing r/D.

Table 2 presents the distributions of $K_{\sigma L}$ at the notch root for different μ values. As shown in Figure 7, the SCF calculated using the empirical equations from reference[2] is smaller than the FEA results up to r/D=0.333 for varying notch depths. Beyond this value, the SCF becomes larger than that obtained using the formula from reference[2]. For shallow notch depths (r/D=0.2 and 0.233), the variations in SCF between the FEA results and the

Table 3. Distributions of $K_{\varepsilon L}$ at the notch root for different μ.

r/D	$K_{\varepsilon L}$ For μ =0.15	$K_{\varepsilon L}$ For μ =0.25	$K_{\varepsilon L}$ For μ =0.35	$K_{\varepsilon L}$ For μ =0.45	$K_{\varepsilon L}$ Ref. [1,2]	% variation of Ref. [1,2] from FEA for μ =0.15	% variation of Ref. [1,2] from FEA for μ =0.45
0.2	2.04605	2.16930	2.30256	2.44412	3.10000	-51.51145	-26.83482
0.233	2.04343	2.16472	2.29603	2.43601	3.00000	-46.81224	-23.15233
0.25	2.03790	2.15749	2.28705	2.42521	2.95000	-44.75714	-21.63890
0.285	2.00222	2.11823	2.24428	2.37878	2.85000	-42.34184	-19.80939
0.333	1.94994	2.06319	2.18595	2.31687	2.75000	-41.03009	-18.69470
0.4	1.91808	2.03067	2.15241	2.28170	2.62000	-36.59511	-14.82644
0.5	1.85481	1.96345	2.08070	2.20536	2.45000	-32.08911	-11.09323
0.667	1.71846	1.81874	1.92706	2.04207	2.32000	-35.00495	-13.61036
1	1.63624	1.73148	1.83431	1.94352	2.15000	-31.39914	-10.62397

formula in reference[2] are -9.3% and -5.81%, respectively, when μ=0.15, and -8.54% and -5.18%, respectively, when μ=0.45. For deep notch depths (r/D=0.667 and 1), the variations are 2.55% and 5.15%, respectively, when μ=0.15, and 2.65% and 5.21%, respectively, when μ=0.45.

Table 3 presents the distributions of $K_{\varepsilon L}$ at the notch root for various μ values. While μ has minimal impact on SCFs for r/D (Figure 7), its influence on SNCFs is significant (Figure 8). Since, Poisson's ratio is a function of strain, therefore it affects more on SNCF than SCF. The differences between the SNCF obtained from finite element analysis and the SNCF calculated using the formula in reference[2] are negative and decrease with increasing μ for the same r/D. For shallow notch depths (r/D=0.2and 0.233), these differences are -51.51% and -46.81%, respectively, when μ=0.15, and -26.83% and -23.15%, respectively, when μ=0.45. For deep notch depths (r/D=0.667 and 1), the differences are -35.00% and -31.39%, respectively, when μ=0.15, and -13.61% and -10.62%, respectively, when μ=0.45.

From this analysis, it is evident that μ influences both $K_{\sigma L}$ and $K_{\varepsilon L}$. Its effect must be accounted for when analysing these factors.

5.0 Variation of In-Plane Stress Factor (T_x) and Stress Component σ_{yy}

The study of crack propagation is important because it helps in understanding the failure mechanisms of materials and structures, ensuring their reliability and safety. Cracks, especially those originating from stress concentrations near notches, can grow over time due to cyclic loading, leading to catastrophic failure if not detected early. By analysing crack growth behaviour, engineers can design materials and components with better resistance to fracture, improving their longevity. Additionally, it aids in the development of non-destructive testing methods to monitor structural integrity in industries like aerospace, automotive, and civil engineering. Understanding crack propagation also plays a crucial role in predicting the lifespan of a component and implementing preventive maintenance strategies.

Three-dimensional (3D) surface fractures are the most prevalent defects in engineering structures and typically lead to catastrophic failure, particularly in aerospace vehicles. The strength of materials is

significantly influenced by the triaxial stress field at the tip of a sharp fracture or fault[20]. The geometry and loading arrangement both affect the initiation and spread of cracks. Understanding the constraint effects along the fracture front, which affect the crack's propagation, is therefore essential. A specimen's geometry and loading configurations are related to the triaxial constraints, which are made up of the in-plane (T_x) and out-of-plane (T_z) constraints. The dimensions parallel to the crack front line have an impact on the out-of-plane constraint, while the dimensions in the normal plane of the fracture front line dominate the in-plane constraint. Since the plane stress condition is considered in this analysis, T_z=0. The ratio of σ_{xx} to σ_{yy} is known as the in-plane stress constraint (T_x).

As suggested by Glinka and Newport[15], Creager and Paris's solution[21] for blunt cracks can be used to estimate stress distribution near the tip of relatively deep notch configurations.

$$\sigma_{xx} = \frac{k_{tn}\sigma_n}{2\sqrt{2}}\left[\left(\frac{1}{2}+\frac{x}{r}\right)^{-1/2} - \frac{1}{2}\left(\frac{1}{2}+\frac{x}{r}\right)^{-3/2}\right] \quad (6)$$

$$\sigma_{yy} = \frac{k_{tn}\sigma_n}{2\sqrt{2}}\left[\left(\frac{1}{2}+\frac{x}{r}\right)^{-1/2} + \frac{1}{2}\left(\frac{1}{2}+\frac{x}{r}\right)^{-3/2}\right] \quad (7)$$

σ_{xx} and σ_{yy} are stress components along the x and y direction, respectively.

σ_n is a nominal stress at the net section (at the notch tip).

From the above equations, it is easy to obtain an expression for the in-plane stress factor

$$T_x = \frac{\sigma_{xx}}{\sigma_{yy}} = \frac{\left(\frac{1}{2}+\frac{x}{r}\right)^{-1/2} - \frac{1}{2}\left(\frac{1}{2}+\frac{x}{r}\right)^{-3/2}}{\left(\frac{1}{2}+\frac{x}{r}\right)^{-1/2} + \frac{1}{2}\left(\frac{1}{2}+\frac{x}{r}\right)^{-3/2}} \quad (8)$$

Xu, Thompson and Topper[16] developed approximate equations to describe the stress field in the region of stress concentration. For finite bodies, the equation in terms of stress, which takes into account the effects of notch radius, the stress concentration factor and length of Ligament (D) on the stress distribution, is presented.

As per Thompson and Topper, the expression for the stress component (σ_{yy} (This is the stress component that is important for fatigue analysis) is given by

$$\sigma_{yy} = f_w g\,\frac{k_{tn}\sigma_n}{2}\left(1+\frac{x}{\alpha r}\right)^{-\frac{1}{2}}\left[1+\left(1+\frac{x}{\alpha r}\right)^{-1}\right] \quad (9a)$$

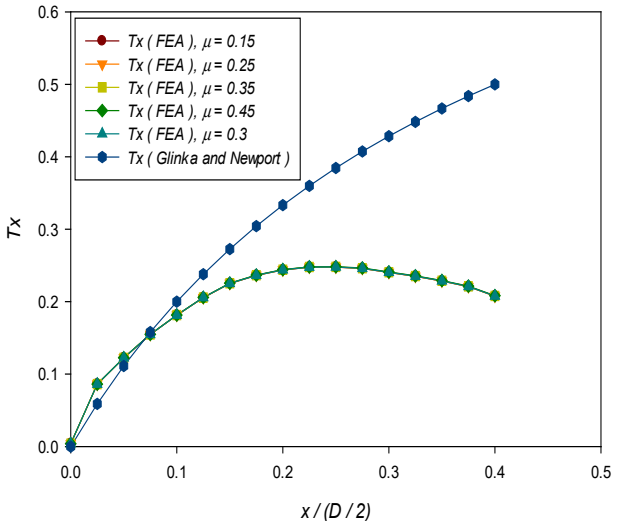


Figure 9. The distribution of T_x near the notch root for different Poisson's ratios (For r/D=0.2, shallow notch).

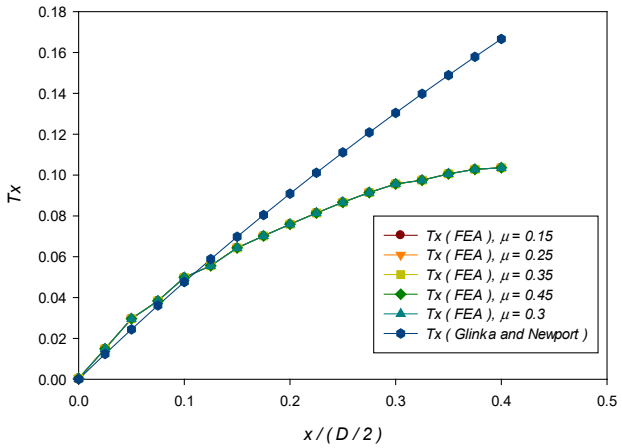


Figure 10. The distribution of T_x near the notch root for different Poisson's ratios (r/D=1, deep notch).

Table 4. The distribution of T_x near the notch root for r/D=0.2.

x/(d/2)	T_x (FEA), μ=0.15	T_x (FEA), μ=0.25	T_x (FEA), μ=0.35	T_x (FEA), μ=0.45	T_x (FEA), μ=0.3	T_x (Glinka and Newport)	% variation of Glinka from FEA μ=0.3 (r/D=0.2)
0	0.00395	0.00394	0.00393	0.00394	0.00393	0.00000	-
0.025	0.08619	0.08619	0.08620	0.08621	0.08620	0.05882	31.75667
0.05	0.12235	0.12237	0.12240	0.12242	0.12238	0.11111	9.21178
0.075	0.15469	0.15472	0.15477	0.15482	0.15475	0.15789	-2.03264
0.1	0.18125	0.18130	0.18137	0.18144	0.18134	0.20000	-10.29275
0.125	0.20547	0.20553	0.20564	0.20574	0.20559	0.23810	-15.81316
0.15	0.22525	0.22533	0.22547	0.22561	0.22540	0.27273	-20.99755
0.175	0.23633	0.23642	0.23659	0.23676	0.23651	0.30435	-28.68339
0.2	0.24383	0.24393	0.24413	0.24433	0.24403	0.33333	-36.59408
0.225	0.24763	0.24773	0.24796	0.24818	0.24785	0.36000	-45.25076
0.25	0.24777	0.24787	0.24813	0.24838	0.24800	0.38462	-55.08750
0.275	0.24592	0.24601	0.24629	0.24655	0.24615	0.40741	-65.51247
0.3	0.24042	0.24049	0.24079	0.24108	0.24064	0.42857	-78.09412
0.325	0.23509	0.23514	0.23545	0.23575	0.23530	0.44828	-90.51496
0.35	0.22854	0.22857	0.22889	0.22921	0.22873	0.46667	-104.02263
0.375	0.22090	0.22090	0.22124	0.22156	0.22107	0.48387	-118.87730
0.4	0.20765	0.20759	0.20794	0.20827	0.20777	0.50000	-140.65452

$$f_w = 1 - \frac{x/r}{(D/2)/r}\left[0.5561 - 0.1123\left(\frac{D/2}{t_1}\right) + \right.$$
$$\left. + 0.005863\left(\frac{D/2}{t_1}\right)^2\right] \quad (9b)$$

$$\alpha = 0.425 + 0.005k_{tn} \qquad t_1 \text{ is notch depth} \quad (9c)$$

$$g = 1 \quad for\ (x/r) < \beta = 0.26(k_{tn} - 1)$$
$$g = 1 + tan\left(\frac{\pi}{2k_{tn}}\right)\frac{(x/r - \beta)}{\gamma} \quad (9d)$$

$$for \quad (x/r) \geq \beta = 0.26(k_{tn} - 1) \quad (9e)$$

$$\gamma = 1.216 + 0.3224k_{tn} \quad (9f)$$

Table 5. The distribution of T_x near the notch root for r/D=1.

x/(d/2)	T_x (FEA), μ=0.15	T_x (FEA), μ=0.25	T_x (FEA), μ=0.35	T_x (FEA), μ=0.45	T_x (FEA), μ=0.3	T_x (Glinka and Newport)	% variation of Glinka from FEA μ=0.3 (r/D=1)
0	0.00042	0.00042	0.00041	0.00041	0.00041	0.00000	-
0.025	0.01487	0.01487	0.01488	0.01488	0.01487	0.01235	17.00383
0.05	0.02964	0.02964	0.02964	0.02964	0.02964	0.02439	17.70707
0.075	0.03836	0.03836	0.03836	0.03837	0.03836	0.03614	5.78556
0.1	0.04980	0.04980	0.04980	0.04980	0.04980	0.04762	4.37474
0.125	0.05557	0.05557	0.05557	0.05557	0.05557	0.05882	-5.85762
0.15	0.06430	0.06430	0.06431	0.06431	0.06431	0.06977	-8.49404
0.175	0.07015	0.07015	0.07015	0.07016	0.07015	0.08046	-14.69465
0.2	0.07590	0.07590	0.07591	0.07591	0.07591	0.09091	-19.76472
0.225	0.08144	0.08145	0.08146	0.08146	0.08145	0.10112	-24.14974
0.25	0.08667	0.08667	0.08668	0.08669	0.08668	0.11111	-28.18855
0.275	0.09145	0.09146	0.09147	0.09147	0.09146	0.12088	-32.16271
0.3	0.09564	0.09565	0.09566	0.09567	0.09566	0.13043	-36.35293
0.325	0.09749	0.09750	0.09751	0.09752	0.09751	0.13978	-43.36000
0.35	0.10059	0.10060	0.10061	0.10062	0.10061	0.14894	-48.03764
0.375	0.10281	0.10283	0.10284	0.10286	0.10283	0.15789	-53.54234
0.4	0.10357	0.10359	0.10360	0.10362	0.10359	0.16667	-60.88583

In Figures 9 and 10, the in-plane stress factor (T_x) is plotted against x/(D/2). The figures are plotted for different values of Poisson's ratios (μ=0.15, 0.25, 0.3, 0.35, 0.45) for shallow and deep notches. It is to be noted that the distributions of T_x ahead of the notch root are merging for these values of Poisson's ratio. This indicates that for both shallow and deep notches, Poisson's ratio is insensitive to in-plane stress calculated by FEA, as shown in Figures 9 and 10.

Tables 4 and 5 present the distribution of in-plane stress factor near the notch root for shallow and deep notches, respectively, and the percentage variation of Glinka's solution from finite element results. A comparison of solutions given by Glinka and Newport and FEA is shown in Figures 9 and 10. For a shallow notch (r/D=0.2), Figure 9 shows the distribution of in-plane stress ahead of a notch root for different Poisson's ratios. For a deep notch (r/D=1), the distribution of in-plane stress

Table 6. Distribution of σ_{yy} near the notch root for shallow notch (r/D=0.2) and deep notch (r/D=1)

x/(D/2)	σ_{yy} (FEA) (μ=0.3) (MPa)	σ_{yy} (FEA) (μ=0.3) (MPa)	σ_{yy} (Glinka) (MPa)	σ_{yy} (Glinka) (MPa)	σ_{yy} (Xu-Thompson) (MPa)	σ_{yy} (Xu-Thompson) (MPa)	% variation of Glinka from FEA (r/D=0.2)	% variation of Xu from FEA (r/D=0.2)	% variation of Glinka from FEA (r/D=1)	% variation of Xu from FEA (r/D=1)
	r/D=0.2	r/D=1	r/D=0.2	r/D=1	r/D=0.2	r/D=1				
0	91.16402	362.86725	99.35529098	343.99981	99.2	344	-8.9852	-8.81486	5.199543	5.199491
0.025	70.54187	345.45618	88.46900741	335.63515	86.226711	329.9241	-25.4135	-22.2348	2.842916	4.496093
0.05	61.80327	325.75931	79.97946644	327.71636	76.376044	316.671	-29.4098	-23.5793	-0.60077	2.78988
0.075	55.92299	312.63504	73.17632091	320.20906	68.63687	304.1684	-30.8519	-22.7346	-2.42264	2.708159
0.1	51.49629	294.20255	67.60271282	313.08227	62.38944	292.3521	-31.2769	-21.1533	-6.41725	0.628955
0.125	47.43765	284.63409	62.95210602	306.30801	57.233723	281.1652	-32.7049	-20.6504	-7.61466	1.21871
0.15	43.81226	269.90457	59.01149602	299.86095	52.900442	270.5566	-34.6917	-20.7435	-11.0989	-0.24159
0.175	41.3884	259.86594	55.62844817	293.71807	49.201933	260.4807	-34.4059	-18.8786	-13.0268	-0.23656
0.2	39.21108	249.69528	52.6911	287.85848	46.00353	250.8963	-34.3781	-17.3228	-15.2839	-0.48101
0.225	37.26622	239.43057	50.11556421	282.26309	43.384794	241.7666	-34.4799	-16.4186	-17.8893	-0.97568
0.25	35.53519	229.10725	47.83773269	276.91451	41.541712	233.0582	-34.6207	-16.903	-20.8668	-1.72451
0.275	34.48967	218.75122	45.80779216	271.7968	39.9003	224.7409	-32.816	-15.6877	-24.2493	-2.73811
0.3	33.068	208.39134	43.98646239	266.89536	38.426523	216.7872	-33.0182	-16.2046	-28.0741	-4.02888
0.325	32.20841	203.21387	42.34235932	262.19678	37.093503	209.1722	-31.4637	-15.1671	-29.025	-2.93206
0.35	31.41198	192.87035	40.85011006	257.68873	35.879738	201.8733	-30.0463	-14.2231	-33.6072	-4.66788
0.375	30.67239	182.54118	39.48898193	253.35984	34.767828	194.8697	-28.7444	-13.3522	-38.796	-6.75382
0.4	29.65629	177.37846	38.24186933	249.19963	33.74354	188.2715	-28.9503	-13.7821	-40.4904	-6.14113

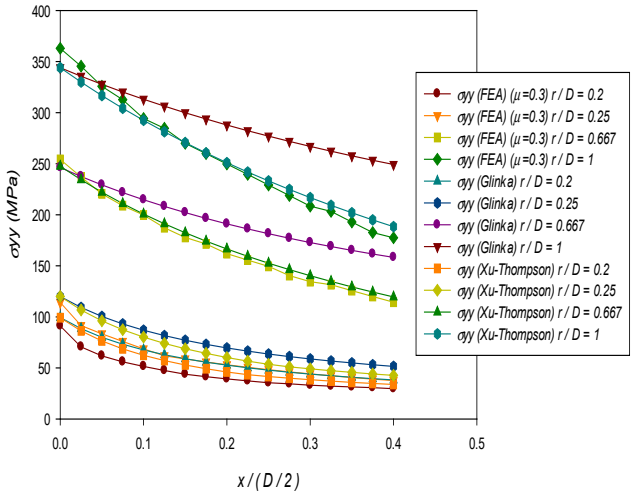


Figure 11. The distribution of σ_{yy} near the notch root for r/D=0.2, 0.25, 0.667 and 1.

is shown in Figure 10. It can be seen that the variation of Glinka and Newport solutions for deep notches from finite element results is less compared to shallow notches at most of the locations. For shallow notch (r/D=0.2), ahead of the notch root, the variation of Glinka's solution from finite element results for μ=0.3 at x/(D/2)=0.2 is -36.59% and at x/(D/2)=0.4, it is -140.65%. For deep notch (r/D=1), the variations are -19.76% and -60.88% respectively.

The comparison of the distribution of stress component (σ_{yy}) by Thompson[16], Glinka and Newport[15] and finite element results for r/D=0.2, 0.25, 0.667 and 0.1 are tabulated in Table 6 and shown in Figure 11. For a deep notch (r/D=1) ahead of the notch root, the variation of Thompson's solution from finite element results is less when compared to Glinka's solution. For a deep notch (r/D=1) at x/(D/2)=0.2, the variation in Glinka and Thompson's solution from finite element results is -15.28% and -0.48% respectively. They are -40.49% and -6.14% respectively when x/(D/2)=0.4. For shallow notch (r/D=0.2), the variations of Glinka and Thompson's solution from finite element result are -34.37% and -17.32% respectively, when x/(D/2)=0.2. They are -28.95% and -13.78% respectively, when x/(D/2)=0.4. Hence for both deep and shallow notches, at most of the locations near the notch root, Xu-Thompson's solution is in close agreement with the finite element results.

6.0 Conclusion

A plate with centrally elongated notch of varying ligament lengths was analysed to study the elastic stress and strain fields under uniaxial tension. The combined influence of Poisson's ratio (μ) and notch depth (r/D) on the stress and strain distributions near the notch root was illustrated on the specimen subjected to axial tensile loading. Analyzing the effect of Poisson's ratio and notch depth on the specimen subjected to bi-axial, torsional, and/or cyclic loading would be a future scope for this research. From the current numerical analysis, the following characteristics were identified.

1. Both k_σ and k_ε decrease, as the distance x increases. The influence of μ on the distribution of k_σ near the notch root is less significant compared to its effect on the distribution of k_ε. However, the impact of μ on also diminishes as the distance x increases. With higher μ values, k_ε increases near the notch root. For shallow notch depths, k_σ and k_ε are higher at the notch root compared to deeper notch depths. At the notch root, and are inversely related to r/D. As r/D (notch depth) increases, the curves of k_σ – x/(D/2) and k_ε – x/(D/2) become flatter.

2. For various r/D values, the distribution of k_ε/k_σ as a function of x/(D/2) decreases with distance up to x/(D/2)=0.275 from the notch root and then increases beyond this point. Both the notch depth r/D and the magnitude of μ influence the k_ε/k_σ - x/(D/2) curve at all points on the plate, except at the notch root. Thus, the distribution of k_ε/k_σ is affected by μ, the r/D value, and the position on the plate. Different locations on the plate exhibit distinct k_ε/k_σ values.

3. As the notch depth (r/D) increases, the values of the stress and SNCFs ($K_{\sigma L}$ and $K_{\varepsilon L}$) near the notch root decrease. Compared to $K_{\sigma L,}$ the $K_{\varepsilon L}$ is more sensitive to variations in μ. Additionally, $K_{\varepsilon L}$ is significantly affected by μ.

4. The in-plane stress factor Tx (by Glinka and Newport[15] increases as the distance ahead of the notch root increases. For the specimen, the variation in the in-plane stress factor by finite element results is less for Glinka and Newport for deep notches than for shallow notches. So for deeper notches, Glinka and Newport provide a good estimate of the in-plane stress factor ahead of the notch root. The in-plane stress factor near the notch

root with varying notch depths can be predicted very well by the finite element analysis.

5. For a deep notch, the variation of the stress component (σ_{yy}) by FEA results is less for Xu-Thompson (up to 6.75%) compared to Glinka's solution (up to 40.49%). For shallow notches ahead of the notch root, the percentage variations of σ_{yy} by Xu-Thompson[16] from FEA up to 23.57%. The variations of the solution by Glinka and Newport[15] are up to 34.69%. This indicates the variation of σ_{yy} with shallow and deep notches, the solution by Xu-Thompson is in close agreement with finite element results.

7.0 References

1. Pilkey W. Peterson's stress concentration factors, 3rd ed. John Wiley & Sons, Inc., Hoboken, New Jersey; 2008.
2. Young WC, Budynas RG. Roark's Formulas for Stress and Strain. 7th ed. Mc. Graw Hill; 2002.
3. Li ZH, Guo WL, Kuang ZB. Three-dimensional elastic stress fields near notches in finite-thickness plates. Int J Solids Struct. 2000; 37:7617-7631. https://doi.org/10.1016/S0020-7683(99)00311-X
4. She CM, Guo WL. Three-dimensional stress concentrations at elliptic holes in elastic isotropic plates subjected to tensile stress. Int J Fatigue. 2007; 29:330-335. https://doi.org/10.1016/j.ijfatigue.2006.03.012
5. Yu PS, G WL, She CM, Zhao JH. The influence of Poisson's ratio on thickness-dependent stress concentration at elliptic holes in elastic plates. Int J Fatigue. 2008; 30:165-171. https://doi.org/10.1016/j.ijfatigue.2007.02.007
6. Zheng Y, Kim CB, Cho C, Beom HG. The concentration of stress and strain in a finite-thickness elastic plate containing a circular hole. Int J Solids Struct. 2008; 45:713-731. https://doi.org/10.1016/j.ijsolstr.2007.08.030
7. Liu H, Deng L, Wang W. 3D stress concentration around circular hole under remote biaxial loading. Int J Mech Sci. 2024; 268:109032. https://doi.org/10.1016/j.ijmecsci.2024.109032
8. Khatawate VH, Dharap MA, Godse A, Balikai VG, Rao AS. Assessment of local stresses and strains using NSSC rules. Lecture Notes in Mechanical Engineering. Singapore: Springer; 2020. https://doi.org/10.1007/978-981-15-4485-9_66.
9. Patel A, Desai CK. Stress concentration around an elliptical hole in a large rectangular plate subjected to linearly varying in-plane loading on two opposite edges. Theor Appl Fract Mech. 2020; 106:102432. https://doi.org/10.1016/j.tafmec.2019.102432
10. Folias ES, Wang JJ. On the three-dimensional stress field around a circular hole in a plate of arbitrary thickness. Comput Mech, 1990; 6:379-391. https://doi.org/10.1007/BF00350419
11. Grant RJ, Lorenzo M, Smart J. The effect of Poisson's ratio on stress concentrations. J Strain Anal Eng Des. 2007; 42:95-104. https://doi.org/10.1243/03093247JSA205
12. Zheng Y. Stress and strain concentration factors for tension bars of circular cross-section with semicircular groove. Eng Fract Mech. 2009; 76:1683-1690. https://doi.org/10.1016/j.engfracmech.2009.03.005
13. Neuber H. Theory of notch stresses: Principles for exact calculation of strength with reference to structural form and material. 2nd ed. Springer, Berlin 1958.
14. Dundurs J. Dependence of stress on Poisson's ratio in plane elasticity. Int J Solids Struct. 1967; 3:1013-1021. https://doi.org/10.1016/0020-7683(67)90026-1
15. Glinka G, Newport A. Universal features of elastic notch-tip stress fields. Int J Fatigue. 1987; 9:143-150. https://doi.org/10.1016/0142-1123(87)90069-7
16. Xu RX, Thompson JC, Topper TH. Practical stress expressions for stress concentration regions. Fatigue Fract Eng Mater Struct. 1995; 18:885-895. https://doi.org/10.1111/j.1460-2695.1995.tb00912.x
17. Altair hyperworks radioss theory manual.
18. Frocht MM. Factors of stress concentration photoelastically determined. Trans ASM. Appl Mech Sect. 1935; 57:A67-74. https://doi.org/10.1115/1.4008610
19. Ling CB. On stress concentration factor in a notched strip. Trans ASME Appl Mech Sec. 1968; 90:833-837. https://doi.org/10.1115/1.3601322
20. Clatterbuck DM, Chrzan DC, Morris Jr JW. The influence of triaxial stress on the ideal tensile strength of iron. Scr Mater. 2003; 49:1007-1011. https://doi.org/10.1016/S1359-6462(03)00490-1
21. Creager M, Paris PC. Elastic field equations for blunt cracks with reference to stress corrosion cracking. Int J Fract. 1967; 3:247-252. https://doi.org/10.1007/BF00182890

Abbreviations

E	Modulus of elasticity
k_σ	Stress ratio
$K_{\sigma L}$	Stress concentration factor.
k_{tn}	SCF from reference
k_ε	Strain ratio
$K_{\varepsilon L}$	Strain concentration factor
r	Notch radius
D	Length of ligament
x	Distance from notch root
σ_{y0}	Uniform stress is applied at the end of the plate.
σ_{yy0}	stress components in the bar at the notch root
σ_{net}	Nominal stress at net section.
ε_{yy0}	strain components in the bar at the notch root
σ_{xx} , σ_{yy}	Stress components
μ	Poisson's ratio
T_x	In-plane stress constraint factor
T_z	Out-of-plane stress constraint factor